Femtosecond Dynamics of Linear Ag_3

Doo Wan Boo, Yasushi Ozaki,† Lars H. Andersen,‡ and W. C. Lineberger*

JILA, University of Colorado and National Institute of Standards and Technology Boulder, Colorado 80309

Received: March 28, 1997; In Final Form: April 23, 1997[⊗]

A femtosecond negative ion−neutral−positive ion charge reversal apparatus has been developed, following the concept of Wöste and Berry, to carry out spectroscopy of transient neutral species along the reaction coordinate. We report studies of the ultrafast dynamics of linear Ag_3 produced by photodetachment of linear Ag_3^-. The background-free time-resolved multiphoton ionization spectra of Ag_3 taken at various wavelengths show a strong probe time and wavelength dependence, indicating important roles both of an intermediate state resonance and the ionization detection window in the time-resolved ionization signal. Based on these results, we speculate on the wavepacket dynamics along the coordinate of the linear-to-triangular rearrangement on the ground state potential energy surface.

Introduction

Femtosecond pump−probe techniques have been extensively used for the real time observation of ultrafast phenomena in the various fields of physics, chemistry, and biology. One of the important applications in chemistry is to transition state spectroscopy, providing real time access to the transition states of elementary chemical reactions.[1] The idea of this technique is to prepare the transition states of the reactions by photoexcitation of stable collision complexes and to follow the evolution of the complexes by using various detection methods such as laser induced fluorescence (LIF), photoelectron spectroscopy, or resonance enhanced multiphoton ionization (REMPI). This technique has successfully been applied to a few bimolecular reactions of alkali halides, mercury halide, and others.[2,3] In another approach pioneered by Neumark,[4−6] the transition states are prepared by photodetachment of negative ions with appropriate geometries. The transition states of neutral bimolecular reactions are in this case produced by vertical photodetachment of stable negative ions that possess a geometry close to that of the transition states. One advantage of this technique is that the ionic complex frequently has a more stable and rigid structure than its neutral counterpart, simplifying the interpretation of the data. Other studies have shown that photodetachment of some negative organic molecules can access the transition states of intramolecular isomerization of the corresponding neutrals.[7−9]

The first application of this technique as a pump step in a femtosecond pump−probe experiment was made by Berry and Wöste in their study[10] of the neutral silver trimer. They used a ∼400-nm pump pulse to prepare a transient linear neutral silver trimer by photodetachment of Ag_3^- and employed a delayed pulse of the same wavelength to interrogate the evolution from linear to triangular form via multiphoton ionization of the evolving Ag_3. They observed that the positive ion signal, named a NeNePo (negative−neutral−positive) signal,[11] increased substantially some 700 fs after the initial photodetachment event and described the increase in terms of a time dependent Franck−Condon overlap factor between the evolving neutral wavepacket and the positive ion potential energy surface (PES) with an equilateral triangular minimum energy structure. The essential features of this interpretation were confirmed by recent theoretical analyses.[12,13]

The apparatus developed[10] in Wöste's laboratory is based on slow ion beam technique for ion accumulation and cooling with the use of a linear quadrupole trap, has a low duty cycle, and may be vulnerable to fluctuations in negative ion beam intensity and to timing jitter between the laser and the ion beams. The advantages of their general approach are substantial, and it was our goal to develop a similar apparatus with a high duty cycle and with the capability of taking into account any fluctuations occurring over extended periods of time in order to take full advantage of the potentially background-free nature of the charge reversal scheme. An enhanced charge reversal apparatus has been developed in our laboratory by using a pulsed ion source and a fast ion beam technique. This apparatus allows us to detect not only the positive ions but also the neutral products with the same efficiency for the purpose of normalization. The use of the fast ion beam technique also allowed us to discriminate completely against any slow positive ions arising from pump or probe ionization of the much higher density background gas molecules. The goal for the new apparatus is to enable the detailed evolution of reacting systems and to provide the capability to obtain transient spectra along an entire complex reaction trajectory.

With this new apparatus, we have first reinvestigated the femtosecond dynamics of the neutral silver trimer. The silver trimer was chosen for the following reasons. The neutral silver trimer is a simple triatomic molecule with a low ionization potential (IP) that can be ionized by two-photon absorption with the laser available. It exhibits a large geometrical evolution after photodetachment, since the ground state of Ag_3 is triangular, while Ag_3^- is linear. The D_{3h} symmetry form of ground state Ag_3 undergoes a strong Jahn−Teller distortion and forms an interesting potential energy surface (PES) with conical intersections, known as a Mexican hat PES,[14] similar to the alkali metal trimers (Li_3, Na_3, etc).[15,16] It is known that these metal trimers undergo pseudorotation, a molecular manifestation of Berry's geometrical phase,[17] around the trough of the Mexican hat surface.[18−20] Therefore, the charge reversal experiment gives the opportunity to investigate the effect of pseudorotation on the dynamics of a wavepacket originating from the linear configuration.

In this paper we describe the new apparatus and report the charge reversal spectra of Ag_3^- taken at various wavelengths

* To whom correspondence should be addressed.
† Permanent address: Department of Chemistry, Josai University, Japan.
‡ Permanent address: Institute of Physics and Astronomy, University of Aarhus, Denmark.
⊗ Abstract published in *Advance ACS Abstracts,* July 1, 1997.

S1089-5639(97)01135-3 CCC: $14.00

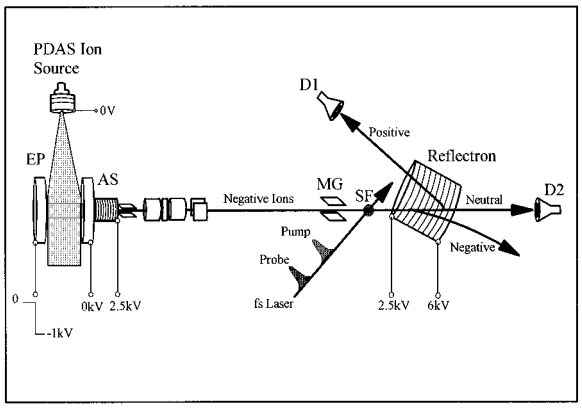

Figure 1. Schematic diagram of the ion beam portion of the charge reversal apparatus.

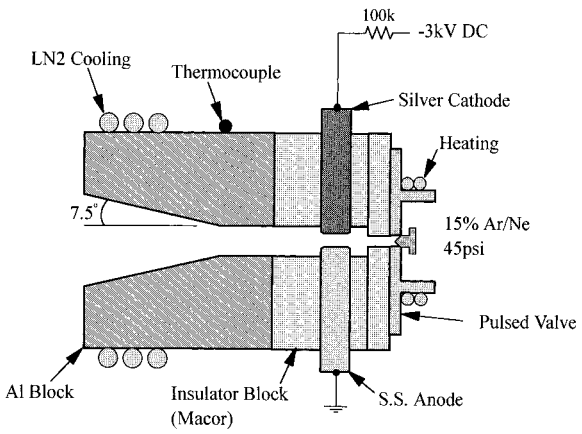

Figure 2. Pulsed discharge Ar^+ sputtering ion source of silver cluster negative ions.

in the region of ~400 nm and ~270 nm. We discuss our preliminary analysis on the ultrafast dynamics in comparison with the previous work of Wolf *et al.*[10] While the general form of the spectra and the overall conclusions are consistent with this work, we find that the form of the time-dependence is very sensitive to the probe wavelength, and a detailed interpretation is both richer and more complex than might be inferred from the work of Wolf *et al.*[10]

Experimental Section

The experiments described here were carried out by incorporating the newly developed charge reversal apparatus with a femtosecond Ti:sapphire laser system. A schematic diagram of the ion beam apparatus is shown in Figure 1. This device is a modification of our tandem time-of-flight (TOF) mass spectrometer, which has previously been employed[21−23] to study the dynamics of I_2^- inside solvent cages. As shown in Figure 1, the apparatus consists of four major components: an ion source, a Wiley-McLaren TOF mass analyzer, a secondary reflection TOF product analyzer, and detectors for product positive ions, neutral photodetachment products, and the parent negative ion beam.

The Ag_3^- ions were produced by a high-pressure pulsed discharge Ar^+ sputtering ion source (Figure 2). A pulsed glow discharge was initiated when a gas pulse containing 15% Ar in Ne, 45 psi total pressure flowed past a −3 kV dc potential from the silver cathode to the stainless steel anode at ground potential. The discharge was quite constant and stable until the gas pulse exited the discharge region. Under normal operating conditions the discharge peak current was ~10 mA, the pulse duration was ~400 μs, and the repetition rate of the pulsed valve was 80 Hz, limited only by the pumping speed in the source chamber. The precursor Ar^+ ions formed in the discharge were accelerated toward the silver cathode by the electric field of ~30 kV/cm, and neutral and anionic silver atoms and clusters, Ag_n and Ag_n^-, were sputtered off the silver cathode surface. The silver cluster ions then undergo collisions with the high-pressure background gas inside the aluminum block maintained at liquid nitrogen temperature. Thus, the silver clusters cooled down considerably and grew in cluster size. The liquid nitrogen cooling was found to be crucial in generating a high-intensity Ag_3^- beam. Finally, the gas mixture containing the silver cluster ions was expanded supersonically through a cone-shaped channel. The typical pressure of the source chamber during the experiment was $\sim 1 \times 10^{-4}$ Torr. About 12 cm below the ion source, a pulsed transverse electric field extracted a small portion of the ions into a Wiley−McLaren TOF mass spectrometer. The ions were accelerated to 3 keV and brought to a temporal and spatial focus ~1.8 m downstream. The pulsed mass gate located just before this focus transmitted only the ions with the mass-to-charge ratio of interest, thus greatly reducing background ion noise. At the spatial focus, the mass-selected negative ions were intersected with a laser beam, and the resulting photoproducts and the precursor ions drifted in a field-free region before entering a single field, reflection TOF mass spectrometer. The photoproducts were mainly neutrals with a small fraction of positive ions. When detecting positive ions, the reflection was set to reverse the trajectories of the positive ions according to their mass-to-charge ratio of the off-axis detector (D1) and deflect the negative precursor ions off the detector as shown in Figure 1. The neutral products passed through the reflectron to reach the in-line detector (D2). Due to the extremely low abundance of positive ions, the detector D1 was run in a single ion counting mode, and the counts of positive ions were typically accumulated for more than 10 000 laser shots. The detector D2 was operated in an analog mode to detect the neutrals simultaneously for normalization purpose. The capability for detecting neutrals was found to be crucial to compensate for negative ion intensity fluctuations; it is also minimized the scatter arising from a small jitter in the temporal overlap of the laser pulses and the ion beam packet that occurred during the measurement.

The femtosecond laser system has been described previously in detail,[23] so a brief description will be given here. The system was a commercial, regeneratively amplified Ti:sapphire laser system. First, a Ti:sapphire oscillator (Coherent Mira Basic), pumped by a 6.5-W Ar ion laser (Coherent Innova 90), produced 750−850-nm, 76-MHz, ~85-fs pulses. These pulses were then stretched to ~150 ps (Quantronix 4800 Stretcher and Compressor), sent into a Nd-YLF pumped regenerative amplifier (Quantronix 4800 Series Ti:sapphire RGA), and subsequently compressed back to ~110 fs. The final output of the laser system consisted of near transform-limited 1-mJ pulse with a 400-Hz repetition rate. The 1-mJ, ~110-fs IR pulse in the 750−850-nm range was converted to the second harmonic (SH) (375−425 nm) and the third harmonic (TH) (250−283 nm) by using 1-mm lithium triborate (LBO) and 1-mm β-barium borate (BBO) crystals, respectively (CSK Model 8315A). Typical outputs are ~300 μJ, ~150 fs for SH and ~100 μJ, ~250 fs for TH. In the case of SH/IR pump−probe, about 50% of the IR output was split to generate the SH and later combined with the other 50% of the IR. Similarly, about 50% of the SH output was split to generate the TH in the case of the SH/TH pump−probe. The collinear pump/probe beam configuration was employed throughout this experiment. The laser beams were both linearly polarized and the directions of the polarization

were parallel to the ion beam. Since the repetition rate of the pulsed valve of the ion source was set to 80 Hz, precise temporal overlap of the ions with the laser pulses was accomplished through the use of a delay generator (Stanford DG 535).

The data collection scheme used in this experiment consisted of two cycles of measurement: background and pump−probe cycles. In the background cycle the positive ion and neutral signals were measured in the absence of one or both laser pulses, namely, pump/probe combinations of on/off, off/on, and off/off. The background ion−neutral ratio (ρ_{bkd}) was then determined in the following manner:

$$\rho_{bkd} = \frac{N^+_{off/on} + N^+_{on/off} - 2N^+_{off/off}}{N^0_{off/on} + N^0_{on/off} - 2N^0_{off/off}}$$

where N^+ and N^0 are the number of positive ions and neutrals and the subscripts off/on, on/off, off/off indicate the status of the pump and probe pulses. The background measurements were averaged over 2000 laser shots and recorded before and after the pump−probe cycle.

In the pump−probe cycle a survey scan was first carried out to determine the general feature of the pump−probe profile and the delay for the maximum signal, or the reference delay. Each pump−probe run contained a set of measurements at seven delay times with typically a 50-fs step, while measurement at the reference delay was performed before and after the run. The reference delay was used to normalize the pump-probe signals at different delays after the background subtraction was made. During the measurement the neutral intensity was monitored at each delay to ensure that the neutral intensity varied less than 10%. The fluctuation in the signal was further reduced by normalizing the positive ion signals by the neutral intensity (calculating the ion−neutral ratio). Typically positive ions were collected at each delay for 1000 laser shots and the neutral intensity was averaged over the same number of laser shots. This run was made more than five times for signal averaging. In subsequent runs, the smallest time delay was set to overlap the largest time delay of the previous run. This provided a way to ensure a good link between the data. After the entire set of delays was scanned, the same procedure was repeated three or more times for further signal averaging.

For the charge reversal studies of Ag_3^-, there are three positive ion channels, Ag_n^+ (n = 1, 2, 3), and a single neutral channel, Ag_3. The positive ions at each channel were counted by using a scaler with a 500-ns gate, and the neutrals were integrated by using an ADC with a 500-ns gate. The ion−neutral ratio $\rho(\Delta t)$ of the true pump−probe signals was calculated in the following way:

$$\rho(\Delta t) = \frac{N^+_{on/on}(\Delta t) - N^+_{off/off}}{N^0_{on/on}(\Delta t) - N^0_{off/off}} - \rho_{bkd}$$

where $N^+_{on/on}(\Delta t)$ and $N^0_{on/on}(\Delta t)$ are the number of positive ions and neutrals when both the pump and the probe pulses are on. The ratio $\rho(\Delta t)$ was finally calculated for each positive ion channel and then scaled by the sum of the ion−neutral ratios of each channel at the reference delay, Δt_{ref}. The final background-free and normalized pump−probe yield, $S_n(\Delta t)$, is given by the following equation:

$$S_n(\Delta t) = \frac{\rho_n(\Delta t)}{\sum \rho_n(\Delta t_{ref})} \times 100(\%), \quad n = 1, 2, 3$$

The scaling of the pump−probe signals by the signal at the reference delay provided a way to do *in situ* normalization and is important when the instrumental sensitivity drifts slowly over extended periods of time.

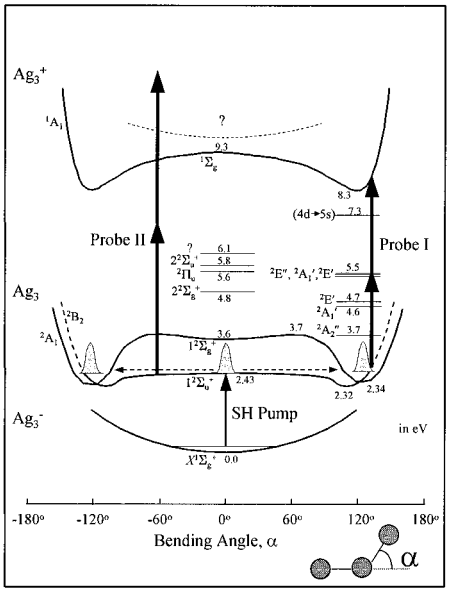

Figure 3. Schematic potential energy curves of Ag_3^-, Ag_3, and Ag_3^+ along the bending coordinate. The energies indicated are drawn from a multiplicity of sources and represent the best present knowledge of this system.

Potential Energy Curves

Figure 3 shows the potential energy curves of Ag_3^-, Ag_3, and Ag_3^+ along the bending coordinate, constructed from combining the previous theoretical[24−35] and experimental[34,36] results on the electronic states of these clusters. The ground state of Ag_3^- is $^1\Sigma_g^+$, a linear structure that is ∼1.3 eV more stable than the equilateral triangular form.[29] In contrast, the ground state of the neutral silver trimer Ag_3 is $^2E'$ in D_{3h} symmetry with an equilateral triangular structure. The degenerate $^2E'$ state splits into $^2B_2$ (obtuse isosceles) and $^2A_1$ (acute isosceles) states due to the strong Jahn−Teller distortion.[24,32] Consequently, the $^2B_2$ state is the global minimum energy state and lies ∼0.02 eV below the $^2A_1$ state.[24,32] The minimum energy state ($^2B_2$) correlates to the $^2\Sigma_u^+$ state of the linear form, which is ∼0.15 eV higher in energy than the $^2B_2$ state. In fact, the $^2\Sigma_u^+$ state is a saddle point along the bending coordinate connecting the minimum energy $^2B_2$ states (see Figure 3). Negative ion photoelectron spectroscopy measurements[36] determined the vertical detachment energy (VDE) for the process

$$h\nu + Ag_3^-(^1\Sigma_g^+) \rightarrow Ag_3(^2\Sigma_u^+) + e$$

and the adiabatic electron affinity for

$$h\nu + Ag_3^-(^1\Sigma_g^+) \rightarrow Ag_3(^2B_2) + e$$

to be 2.43 and 2.32 eV, respectively. The same experiments determined[36] the dissociation energy for $Ag_3 \rightarrow Ag_2 + Ag$ to be ∼1 eV. The linear structure that correlates to the $^2A_1$ state (the other Jahn−Teller partner of $^2B_2$) has $^2\Sigma_g^+$ symmetry, is located ∼1.2 eV above the $^2\Sigma_u^+$ state, and forms a minimum in a shallow well of ∼0.1-eV depth.[24] Gantefor and co-workers measured[34] the VDE to the higher lying $^2\Sigma_g^+$ Ag_3 state to be 3.62 eV, consistent with the theoretical prediction.

Walch[33] has calculated excitation energies from the $^2B_2$ state to several high-lying D_{3h} electronic states of Ag_3. The calculated excitation energies were 1.42 eV for $^2A_2''$, 2.28 eV for $^2A_1'$,

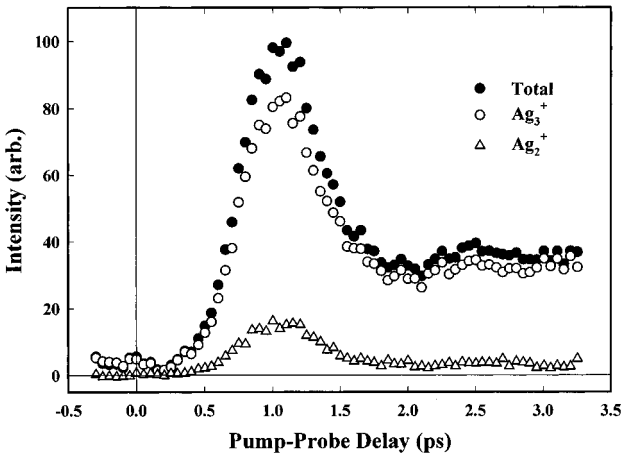

Figure 4. Ag_3^- charge reversal spectrum obtained with a 410-nm photodetachment (pump) and 410-nm REMPI (probe) excitation.

2.4 eV for $^2E'$, 3.26 eV for $^2E''$, 3.19 eV for $^2A_1'$, 3.23 eV for $^2E'$, and 4.94 eV for Ag_3 4d → 5s. The $^2E'' \leftarrow {}^2B_2$, $^2A_1$ transition (∼3.4 eV) has been observed experimentally by Duncan and co-workers.[37−39] Several matrix isolation studies on the optical absorption of neutral silver trimers have also been reported and they observed several absorption bands in the 200−500-nm region.[40,41] For the high-lying linear electronic states, Gantefor and co-workers[34] carried out photoelectron spectroscopy on Ag_3^- and reported the VDEs (4.83, 5.57, 5.80, 6.10 eV). They assigned the first three VDEs to $2^2\Sigma_u^+$, $1^2\Pi_u^+$, and $2^2\Sigma_u^+$ states of the neutral Ag_3 by comparison with theoretical VDE values.

For Ag_3^+, the ground state is an equilateral triangular structure ($^1A_1$) with D_{3h} symmetry, located ∼6 eV (IP) above the $^2B_2$ state of the neutral Ag_3.[25,28,30,37] The linear $^1\Sigma_g$ state is predicted to lie ∼1 eV higher than the $^1A_1$ state.[30] The reported[28] dissociation energy for $Ag_3^+ \rightarrow Ag_2^+ + Ag$ is ∼2.8 eV. No calculations on the excited states of Ag_3^+ have yet been reported, but triplet states such as $^3\Pi_u$ (linear) and $^3E''$ (triangle) are expected at higher energies, in analogy with a calculation[42] on Cu_3^+. Figure 3 summarizes the available information on the relevant Ag_3 surfaces.

Results and Discussion

The longest wavelength radiation capable of photodetaching Ag_3^- is the second harmonic radiation from the Ti:sapphire laser at ∼400 nm. Absorption of one photon of this color produces exclusively Ag_3 on the ground state PES. Accordingly, we have carried out detailed charge reversal studies with this (SH) pump radiation and then employed IR fundamental (∼800 nm), second harmonic (∼400 nm), and third harmonic (∼270 nm) multiphoton ionization probe photons. As each of these three cases present different issues, they are discussed separately before drawing overall conclusions.

1. One-Color Pump-Probe: SH Pump−SH Probe. Figure 4 shows a typical charge reversal spectrum of Ag_3^- taken with 410-nm (3.02 eV) photodetachment (pump) and photoionization (probe) pulses; while there is semiquantitative information on the approximate cross sections, the positive ion signal here is normalized to 100 at its maximum value. The pump and probe laser intensities in the interaction region were $\sim 1 \times 10^{10}$ W/cm^2, and the maximum positive ion signals were typically ∼0.2 ions per a single pump-probe pulse. So, ∼25 000 total number of pump−probe pulses were used for the integration and averaging of the positive ion signals to give the spectrum shown in Figure 4 (refer to the Experimental Section about the integration and averaging scheme used). Since the lowest VDE of Ag_3^- and

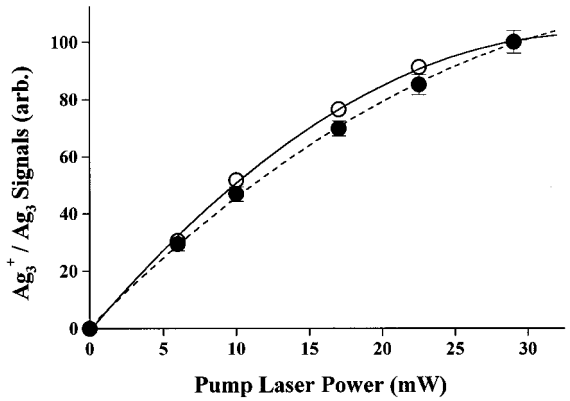

Figure 5. Pump power dependence of the Ag_3 yield (−○−) with the probe laser off, and the Ag_3^+ ion yield (- - -●- - -) at $\Delta t = 1$ ps and with a fixed probe intensity, obtained with a 410-nm pump and 410-nm probe.

the adiabatic IP of Ag_3 are ∼2.4 and ∼6 eV, respectively, photodetachment by one 410-nm pump photon is sufficient to prepare the Ag_3 neutrals, whereas two (or more) 410-nm probe photons are required to ionize the neutrals. This two-photon ionization scheme is depicted as Probe I in Figure 3. Notice that the total energy of two 410-nm photons is close to the adiabatic IP of Ag_3. Among the possible charge reversal products, Ag_n^+ (n = 1, 2, 3), Ag_3^- was always the dominant product, comprising 80−90% of the total ion yield, depending on how tightly the laser beams were focused in the interaction region. The Ag_2^+ product comprised virtually all of the other ionic products, but there was a detectable trace of Ag^+. As shown in Figure 4, the total ion yield remains less than 5% for Δt < 300 fs, then it increases gradually and reaches a maximum (100%) at $\Delta t = \sim 1$ ps. After ∼1 ps, the total ion yield decays gradually to a minimum (∼30%) at $\Delta t = \sim 2$ ps and recovers slightly to ∼35% and stays more or less constant for 200 ps (which was the longest time delay used in the experiment). The strong time dependence of the charge reversal signal confirms both significant evolution of the neutral wavepacket and high selectivity in detection depending on where the neutral wavepacket was located on the PES. The observation that Ag_2^+ and Ag_3^+ exhibit the same time dependence suggests strongly that the Ag_2^+ signal originates primarily from the dissociation of Ag_3^+ as a result of additional probe photon absorption. The Ag_2^+ fragment ion must be the result of at least three 410-nm probe photon absorptions in order to reach the 2.8 eV threshold[28] for $Ag_3^+ \rightarrow Ag_2^+ + Ag$. The small peak at $\Delta t = 0$ ps is due to interference between pump and probe pulses when they overlap in time in the collinear beam geometry. The maximum of the interference was used to determine the time zero (Δt = 0 ps) within an uncertainty of ∼50 fs.

It is critical that we have definitive information concerning which electronic states of Ag_3 are accessed by the 410-nm pump photon, if we are to analyze properly the ensuing wavepacket dynamics. If single photon photodetachment at 410 nm were the only significant neutral production channel, then Ag_3 would be formed only in the $^2\Sigma_u^+$ state (see Figure 3). However, if two-photon photodetachment makes a significant contribution, then most of the linear neutral states shown in Figure 3 would be accessible. To clarify the issue, we have determined the **pump** power dependence of both the neutral and the positive ion signals, the latter being obtained with a fixed probe power. In order to test for this possibility, we have carried out a careful study of the dependence of both the neutral and positive ion signals on the photodetachment (pump) laser power. Figure 5 shows the dependence of the neutral signal on **pump** power, together with the dependence of the Ag_3^+ ion signal at $\Delta t = 1$

ps (peak) on **pump** power at a **fixed probe** laser intensity. The neutral yield shows a slight saturation behavior at high pump power ($\sim 1 \times 10^{10}$ W/cm^2), and the Ag_3^+ ion signal follows the same trend (Figure 5). The same trend of the positive ion yield indicates that the 410-nm probe pulse is able to ionize the ground state neutrals efficiently. Therefore, the features of the spectrum in Figure 4 represent the evolution of the neutral wavepacket on the **ground state** PES.

The features in Figure 4 are qualitatively very similar to the results of Wolf *et al.*,[10] with the exception of a slight shift in the time of peak signal (~1 ps vs ~800 fs) and a much lower baseline in our spectrum. It should be emphasized that the spectra shown in this paper contain only the true pump−probe yield after all the background ions were taken into account (refer to the Experimental Section). The origin of the slight peak shift between our results and theirs is unclear, but the peak positions in the spectra of Wolf *et al*. might be slightly shifted by their much higher background levels. The time dependent Ag_3^+ signal by Wolf *et al*. was interpreted in terms of changes in the Franck−Condon overlap factor between the ground state PES of the neutral and the positive ion along the rearrangement coordinate, assuming nonresonant two-photon ionization for the SH probe. The essential features of this interpretation were later supported by MD simulations by Jeschke *et al*.[12,13]

While the scenario developed by Wolf *et al*. describes the trends of their spectra, some of the details should be reconsidered. First, their assumption of nonresonant two-photon ionization was not tested, so the possibility of intermediate state resonances playing a significant role in determining the shape of the positive ion signal needs to be considered. Second, as mentioned above, the total energy of two SH photons (390−420 nm) is quite close to the adiabatic IP of Ag_3 (~6 eV), and the vertical ionization energies along the bending coordinate vary from ~7 eV for the linear form to ~6 eV for the equilateral triangle form (see Figure 3). Therefore, the ionization detection window of the SH probe pulse would be limited to the region of triangular form, and the extent of that window could be strongly dependent on the SH probe wavelength. The low positive ion signal near $\Delta t = 0$ (i.e., linear configuration) could be due to the inaccessibility of Ag_3^+ by two-photon ionization of the SH probe rather than a result of poor Franck−Condon overlap as suggested by Wolf *et al*. The relative intensities of the positive ions inside the ionization detection window may to a good approximation be determined by the Franck−Condon overlap factor. Third, the wavelength dependence of the time location of the maximum signal (800 fs for 420 nm, decreasing to 500 fs for 390 nm) was explained in terms of greater bending excitation of Ag_3 when it was prepared by a higher energy photon (390 nm). The greater excitation would then result in earlier arrival in the detection window in the triangular region. However, this explanation appears unlikely because the SH pump photon energies (~3 eV) are well above the threshold of photodetachment (~2.4 eV), and the vibrational state distribution of Ag_3 will be determined mainly by the (photon energy independent) Franck−Condon overlap factors between the negative ion and the ground state neutral PES. The shifts of the peak positions with wavelength would seem to be more likely the result of a wavelength dependence in the probe process, arising from intermediate state resonances and the change in the location of the ionization detection window as the total energy changes.

In order to test our interpretation, we have taken the charge reversal spectra of Ag_3^- at three other wavelengths (396, 404, 415 nm). Figure 6 shows the spectrum taken with 396-nm pump and 396-nm probe radiation, normalized to 100% at the maximum of the total ion signal. The positive ion yield was about five times less than in the case of 410-nm pump−probe, with the consequence that the pump and probe beams had to be slightly more focused than 410 nm in order to have good statistics. As shown in Figure 6, the features of the spectrum are less time-dependent than in the case of 410-nm pump−probe. The maximum of the Ag_3^+ signal is located at Δt = ~600 fs, and then the signal decreases slowly to ~30% at Δt = 10 ps. The Ag_2^+ signal peaks at Δt = ~900 fs, with a shoulder at Δt = ~600 fs. The different type of the Ag_2^+ signal, compared to Ag_3^+ suggests that at this color the Ag_2^+ ions were formed not only from the dissociation of Ag_3^+ but also by other mechanisms, such as the ionization of the neutral fragment Ag_2 produced from the dissociation of electronically excited Ag_3 due to two-photon detachment. This observation of such less time-dependence in the positive ion yield and the earlier peak (~600 fs) with a 396-nm probe is in general agreement with the results of Wolf *et al*. The shift of the peak position could be due to changes in the size of ionization detection window as the probe wavelength changes. It is conceivable that the 396-nm probe can access the configurations closer to the linear form than the 410-nm probe, resulting in the earlier peak (see Figure 3). On the other hand, if nonresonant two-photon ionization occurred in the triangular form, the positive ion yield near the ionization threshold should change (probably increase) only gradually as the probe wavelength becomes shorter. The strong wavelength dependence of the positive ion yield suggests that intermediate state resonances play a role and could also be responsible for the observed shifts of the peak positions. A third possibility is the competition between two-photon ionization and three-photon ionization as the two-photon REMPI cross section decreases (in the case of 396-nm probe), evidenced by the relatively high positive ion yield (~50%) near $\Delta t = 0$ ps (where at least three-photon absorption is necessary to ionize the neutrals). In the case of three 396-nm photon ionization (~9.4-eV total energy), only the Franck−Condon overlap factor, not the ionization window, might determine the time dependence of the positive ion yield. Additionally, some of the Ag_3 neutrals might be formed in excited states by two-photon detachment, as suggested by the different shapes of the Ag_2^+ and Ag_3^+ signals at this wavelength. The charge reversal spectrum at 396-nm probe could well contain contributions from many different mechanisms proposed above, and more systematic investigation is required before a definitive conclusion can be reached.

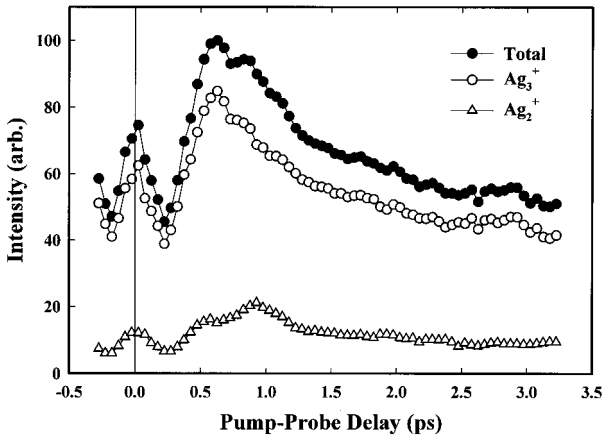

Figure 6. Ag_3^- charge reversal spectrum obtained with a 396-nm photodetachment (pump) and 396-nm REMPI (probe) excitation.

The charge reversal spectra of Ag_3^- were also taken at two other probe wavelengths derived from the SH of the laser, 404 and 415 nm. The general shapes of the time dependence for each color was quite similar to the 410-nm probe, but the

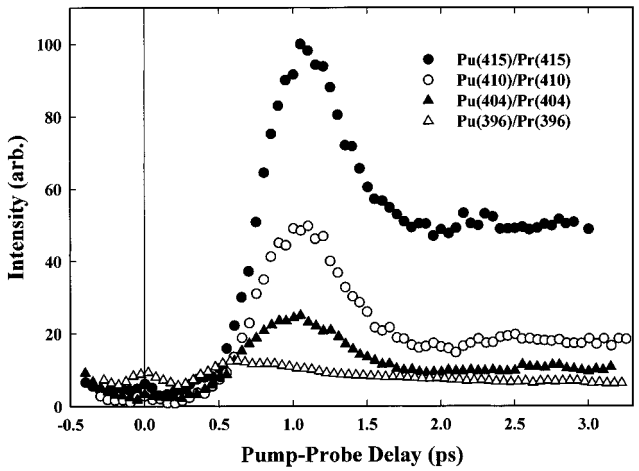

Figure 7. Normalized total positive ion yield at 396-, 404-, 410-, and 415-nm pump−probes. The maximum yield of the 415-nm pump−probe was set to be 100.

magnitude of the signal exhibited a strong wavelength dependence. For both wavelengths, the maximum of the positive ion yield occurred at $\Delta t = \sim 1$ ps, and there was a plateau for $\Delta t \geq \sim 2$ ps, very similar to the 410-nm case described earlier. The Ag_2^+ signal exhibited the same time dependence as Ag_3^+. Figure 7 summarizes the relative **probe** ion yield for four SH wavelengths, normalized to the maximum at 415 nm. The relative two-photon ionization cross sections were obtained by assuming that the cross section for the photodetachment step was wavelength independent, estimating the laser intensities and the number of negative ions in the interaction volume. Since this procedure does not take into account the inhomogeneous spatial distribution of the laser pulses and ions, it allows only a semiquantitative interpretation. Nevertheless, the two-photon probe ionization cross section shows a strong wavelength dependence. The total positive ion yield for $\Delta t \geq \sim 500$ fs increases as the probe wavelength becomes longer. At the same time, the intensity of the plateau region compared to the maxima also increases slowly (∼10% for 404 nm increasing to 50% for 415 nm). This trend in the ionization efficiency is opposite to the general trend of photoionization efficiency near threshold: the ionization efficiency rises slowly as the photon energy increases. The opposite behavior of ionization strongly suggests an intermediate state resonance at longer SH wavelength (probably longer than 415 nm in the triangular region), so that the ionization efficiency decreases as the wavelength becomes shorter. Such intermediate state resonance could also change the time dependence of the positive ion yield. The presence of any triangular intermediate states for Ag_3 near ∼3 eV above the ground state has not yet been confirmed experimentally. Only one REMPI study on Ag_3 by Duncan, *et al.*[37,38] was able to locate a $^2E''$ state near 3.4 eV. The *ab initio* calculation by Walch[33] predicted at least three states ($^2E''$, $^2A_1'$, $^2E'$) near 3.2 eV, close to the energy of one SH photon (see Figure 3). Interestingly, in matrix isolation studies of Ag_3 using Ar and Kr matrices several absorption bands were observed in the 380−500-nm region (for example, 386, 402, 423, 444, and 492 nm for Ar matrix).[40,41] The corresponding gas phase wavelengths will be somewhat shorter due to the matrix effects (386 nm in Ar matrix vs 365 nm in the gas phase).

Our interpretation on the ultrafast dynamics of the ground state neutral silver trimer is in general similar to that of Wolf *et al*. The neutral wavepacket is initially formed in a linear configuration as a coherent superposition of the eigenfunctions in the transition state by the vertical Franck−Condon photodetachment process of the SH pump pulse. The internal state distribution of the neutral wavepacket is more or less constant for the four SH wavelengths used. The linear neutral wavepacket evolves slowly along the bending coordinate due to an almost flat PES near the linear form, and the positive ion yield stays low because the vertical ionization energy exceeds two SH-photon energies in this region. Once the neutral wavepacket reaches parts of the PES with steeper slope, it starts to accelerate toward the global minimum obtuse isosceles, and the positive ion yield increases as the neutral wavepacket reaches the ionization detection window. After the obtuse isosceles minimum, the wavepacket decelerates, passes the equilateral triangular region and the acute triangular region, and finally reaches the classical turning point. In this region, which is inside the detection window, the positive ion yield grows quickly, and reaches the maximum ($\Delta t = \sim 1$ ps, probably near the equilateral triangular configuration) at the point where the Franck−Condon factor between the wavepacket, the intermediate state PES, and the positive ion PES is the greatest. After the classical turning point, the positive ion yield further decreases and reaches a constant level as the neutral wavepacket dephases extensively and randomizes inside the Mexican hat PES. Since the Mexican hat PES is highly anharmonic, and since the neutrals are vibrationally excited, the vibrational modes mix among the internal degrees of freedom, and consequently the neutral wavepacket quickly dephases. It starts to undergo pseudorotation through the three equivalent obtuse triangular structures around the trough of the PES, similar to the cases of alkali-metal trimers.[16] For Na_3, it has been reported[20] that internal energy only slightly in excess of the zero point energy can be randomized in less than 500 fs. The cusplike feature at the equilateral triangular configuration also helps to prevent the neutral wavepacket from reversing its trajectory and may well be the reason that recurrences are not observed in the positive ion signal. Instead, the excited Ag_3 molecules appear to be trapped in the Mexican hat region of the PES for more than 200 ps.

2. Two-Color Pump-Probe: SH Pump−TH Probe. In this section we discuss the charge reversal spectra taken with SH pump and TH probe wavelengths. In this case, the total energy of two TH photons is well above the ionization threshold throughout the entire reaction coordinate space, and the [1 + 1] REMPI occurs via different intermediate states, while the photodetachment pump process is identical to the one-color case. With this scheme the role of the detection window is expected to be minimal, and intermediate state resonances should be the important factor that determines the features of the ionization spectra. This ionization scheme is labeled Probe II in Figure 3. The spectrum shown in Figure 8 was obtained with 410-nm pump and 273-nm probe radiation, normalized to 100% at the maximum of the total ion yield. The time zero in the SH pump−TH probe was determined within an uncertainty of ∼100 fs by finding the time zero in the charge reversal spectra of AgO^- and Ag_2^-. As shown in Figure 8, the features of the spectrum are quite different for the 410-nm pump/410-nm probe case (Figure 4). The total ion yield peaks at $\Delta t = 0$, decreases slowly to ∼90% at $\Delta t = \sim 400$ fs, forms a shoulder feature, and then drops rapidly to a minimum (∼10%) at $\Delta t = \sim 1.5$ ps. After ∼1.5 ps, the total ion yield recovers slowly to ∼20% and then stays constant for at least 50 ps (the longest time delay used in the experiment). Strikingly, the peak intensity near $\Delta t = 0$ ps is ∼30 times higher than that of the 410 nm probe, and even at the plateau region ($\Delta t \geq \sim 2$ ps) the yield of the 273-nm probe is higher than the peak yield of the 410-nm probe. The pump and probe beams had to be quite defocused in the interaction region to avoid saturation of the ion detector. The

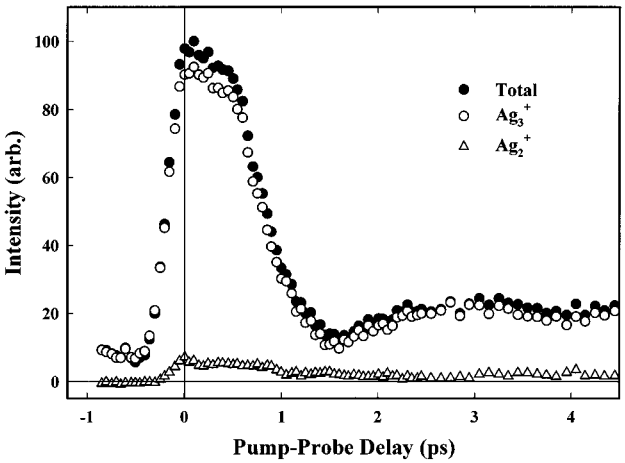

Figure 8. Ag_3^- charge reversal spectrum obtained with a 410-nm photodetachment (pump) and 273-nm REMPI (probe) excitation.

Ag_2^+ signal is less than 10% of the total ion yield and shows similar time dependence as the Ag_3^+ signal, suggesting that the Ag_2^+ ions were again formed from dissociation of the Ag_3^+ ions.

To confirm that the neutral wavepacket being ionized by probe pulse was formed on the ground state PES and to determine how many photons were absorbed from the 273-nm probe pulse, we measured the pump and probe power dependence of the neutral and the positive ion yield. Figure 9a shows the pump power dependence of the neutral yield with the probe laser off and the Ag_3^+ ion yield at $\Delta t = 300$ fs and 3 ps with a fixed probe intensity. Both neutral and positive ion yield show a linear dependence on the photodetachment (pump) laser power, indicating that the neutral wavepacket is indeed formed on the ground state PES and then ionized by the probe pulse. This finding also confirms that the peak near $\Delta t = 0$ and the plateau at $\Delta t \geq 2$ ps have the same origin and could represent the evolution of the ground state neutral wavepacket. The positive ion signal shows a quadratic **probe** power dependence at both $\Delta t = 300$ fs and 3 ps (Figure 9b), indicating that the positive ion yields both at the peak and at the plateau are due to two-photon ionization with the 273-nm probe pulse. The observation of the peak near $\Delta t = 0$ rather than $\Delta t = \sim 1$ ps (the 410-nm probe case) is remarkable, considering the fact that the neutral wavepacket was prepared by the same pump wavelength (410 nm). In addition to the maximum near $\Delta t = 0$ ps, the low positive ion yield (~30%) at ~1 ps where the maximum occurs at 410-nm probe suggests that the intermediate state in the 273-nm probe case could have a linear minimum energy configuration. The existence of such a linear intermediate state is also supported by the observation of the lower relative intensities in the plateau region (~20%), compared to the case of the 410-nm probe (~35%), since the probe via the linear intermediate state would make less access to the neutrals trapped in the triangular well at longer time delays.

In order to study the dependence of the spectra on the wavelength of the TH probe, we obtained additional spectra with 415-nm pump−277-nm probe and 404-nm pump−269-nm probe pulses. Figure 10 shows the total ion yield for the 277-, 273-, and 269-nm probes, normalized such that 100 represents the maximum of the total ion yield for 415-nm pump−415-nm probe (Figure 7). The relative intensity factors were again obtained in the same way as in the earlier case of SH pump−SH probe. The first thing to notice is the greater ionization efficiency of the TH probe compared to the SH probe, indicating a large cross section for intermediate state excitation by the TH probe. Moreover, the positive ion yield in the TH

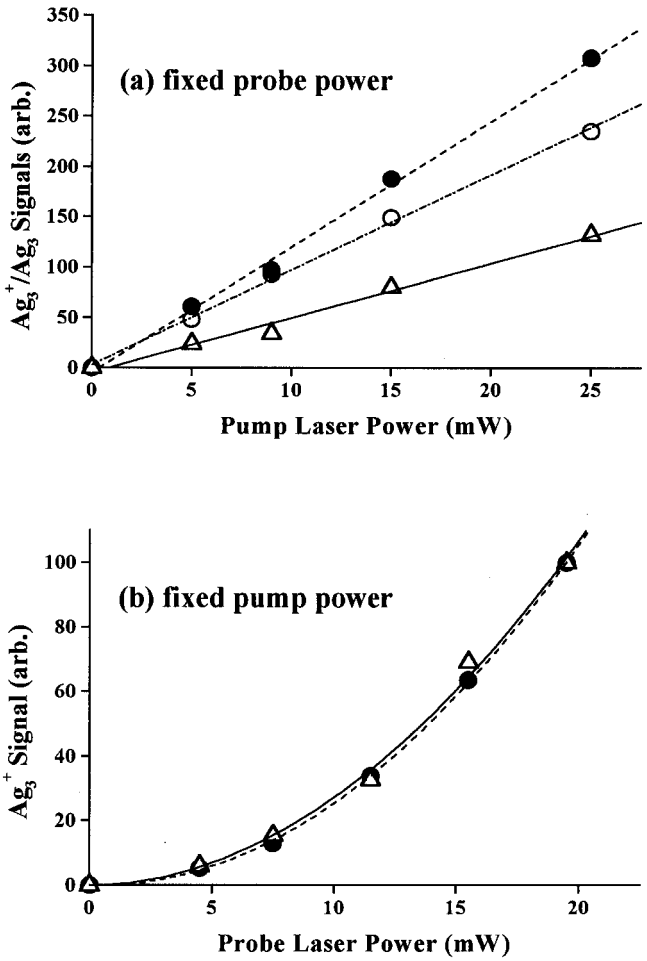

Figure 9. (a) **Pump** power dependence of the neutral yield (−○−) with the probe laser off, and the Ag_3^+ ion yield at $\Delta t = 300$ fs (- - -●- - -), 3 ps (−Δ−), and with a fixed probe intensity; (b) the **probe** power dependence of the Ag_3^+ ion yield at the same delays and with a fixed pump intensity in the case of the 410-nm pump−273-nm probe.

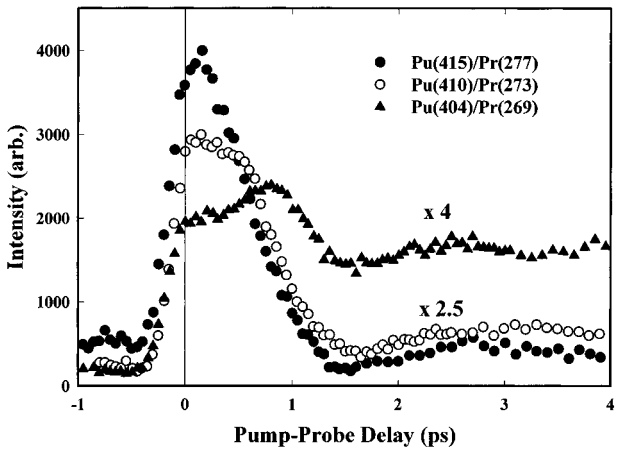

Figure 10. Normalized Ag_3^- charge reversal spectrum obtained with ~410-nm photodetachment (pump) excitation and 277-, 273-, or 269-nm REMPI (probe) excitation. 404−269-nm, 410−273-nm, and 415−277-nm pump−probes. The intensity scale is such that the maximum of the total ion yield of the 415-nm pump−415-nm probe is 100.

probe depends strongly on the TH wavelength. Second, the time dependence of the positive ion yield in the TH probe is sensitive to the probe wavelength. The details of the charge reversal spectra for 415-nm pump−277-nm probe are as follows: the general features of the spectrum are more or less similar to the case of 410-nm pump−273-nm probe but the peak near $\Delta t = 0$ ps is narrower. After the peak near $\Delta t = 0$, the

total ion yield decays to a minimum (~5%) at $\Delta t = \sim 1.5$ ps, then recovers slowly to ~10%, and then remains constant for at least 50 ps. The Ag_2^+ signal was less than 5% of the total ion signal and showed the same time dependence as the Ag_3^+ yield. For 404-nm pump−269-nm probe, the positive ion yield was about an order of magnitude smaller than the case of 415-nm pump−277-nm probe, and the general features of the spectrum were also different from the latter. As shown in Figure 10, the total ion yield forms a maximum at $\Delta t = \sim 800$ fs with a shoulder (~80%) near $\Delta t = 0$ ps and decays to a minimum (~60%) at $\Delta t = \sim 1.5$ ps. After 1.5 ps, the ion yield recovers slowly to form weak and broad features (~70%) at $\Delta t = \sim 2.5$ ps and then stays more or less constant at ~65% for 50 ps. The weak Ag_2^+ signal showed the same general behavior.

The charge reversal spectra for the three different probe wavelengths show the following trend: as the wavelength becomes shorter, the positive ion yield decreases, broadens in time, and the peak position shifts to later times. At the same time the relative intensities of the plateau region increases (10% for 277 nm vs 65% for 269 nm). These features are consistent with the involvement of a **linear** intermediate state in the TH [1+1] REMPI step. Although it is not compelling without accurate characterization of the intermediate state PES, our interpretation is that the 277 nm excites a state near the bottom of the intermediate state minimum, sampling primarily near linear configurations on the ground state PES. However, the 269 nm could reach vibrationally excited levels of the intermediate state covering a wider range of nuclear configurations, including some triangular forms. A greater positive ion signal at $\Delta t = \sim 800$ fs than near $\Delta t = 0$ in the case of the 269-nm probe could be due to the fact that the wavefunction of the vibrationally excited state has a maximum amplitude at the turning point (near the bent form). Furthermore, the reason for a higher positive ion yield at the 277-nm probe compared to the case of the 269-nm probe could be that the Franck−Condon overlap between the linear wavepacket and the lower vibrational level of a linear intermediate state would be greater. Another interesting observation is that the minimum in the total positive ion yield for all three probe wavelengths is located at $\Delta t = \sim 1.5$ ps. Considering the strong wavelength dependence of the [1+1] REMPI process, the origin of the minima at the same time delays should be related to the dynamics of the neutral wavepacket on the ground state PES. Moreover, the positive ion yield decreases monotonically after the peak near $\Delta t = 0$ ps until the minima at $\Delta t = \sim 1.5$ ps. Our tentative interpretation is, though the exact origin is still unclear, that ~1.5 ps might correspond to the time for a slow component of the wavepacket to travel from the linear form to outside the ionization window (probably near the classical turning point).

3. Two-Color Pump-Probe: SH Pump−IR Probe. Finally, the charge reversal spectra of Ag_3^- were also taken with a SH pump−IR probe scheme (415−830 nm, 410−820 nm, 404−808 nm, 396−792 nm). Surprisingly, the spectra were quite different from either the SH and TH probe spectra. There is a peak near zero delay and a rapid decay of signal. To better understand the origin of this signal, power dependence studies were again carried out for both pump and probe pulses. The positive ion yield showed a **quadratic** dependence on the pump power, while the neutral yield showed the same (linear with some saturation) pump power dependence shown in Figure 5. This result is consistent only with the conclusion that there is a small two-photon photodetachment component producing some Ag_3* (the excited state silver trimers) and the IR probe ionizes exclusively the excited state neutrals, not the dominant ground state Ag_3. This surprising result emphasizes the necessity of careful power dependence studies at all wavelengths. More systematic studies will be required before the state(s) involved can be identified.

Conclusions

A new 100-fs resolution negative ion−neutral−positive ion charge reversal apparatus using a pulsed ion source and a fast ion beam technique is described; the first application is to the ultrafast bending dynamics of linear Ag_3. We have measured the background-free charge reversal spectra of Ag_3^- using single photon photodetachment as a pump step and [1+1] REMPI of Ag_3 as a probe step at various wavelengths. We find a strong probe wavelength dependence of the spectral features such as the time dependence, the peak positions, and the positive ion yield. The wavelength dependence has been interpreted in terms of the intermediate state resonances and the changes in the detection window, extending the interpretation of Wolf *et al*.[10] We discuss the femtosecond dynamics of the neutral silver trimer in comparison with their results. Although more systematic studies are necessary in order to answer the details of the dynamics, it is quite apparent that the charge reversal scheme has the potential of revealing the details of the dynamics by accessing different intermediate and positive ion states in the probe.

The charge reversal scheme is a general technique for investigating the time evolution of a coherent, nonequilibrium state of neutrals, as suggested by Wolf *et al*. With tunable femtosecond probe pulses, one can study the time evolution of many unstable radicals. It will be possible to study many fundamental rearrangement processes as a function of location on the reaction coordinate, including ring opening, ring closing, hydrogen atom transfer in simple organic molecules and clusters, and transition states. This technique takes us another step on the path to realize the goal of observing evolving structures along a reaction coordinate.

Acknowledgment. We gratefully acknowledge the support from the National Science Foundation under Grants PHY95-12150 and CHE97-03486. We also acknowledge Dr. Albert Stolow for stimulating discussions on the results of this work. L.H.A. was supported by the JILA Visiting Fellow program.

References and Notes

(1) Zewail, A. H. *Faraday Discuss. Chem. Soc.* **1991**, *91*, 207.
(2) Mokhtari, A.; Cong, P.; Herek, J. L.; Zewail, A. H. *Nature* **1990**, *348*, 225.
(3) Dantus, M.; Bowman, R. M.; Gruebele, M.; Zewail, A. H. *J. Chem. Phys.* **1989**, *91*, 7437.
(4) Weaver, A.; Metz, R. B.; Bradforth, S. E.; Neumark, D. M. *J. Chem. Phys.* **1990**, *93*, 5352.
(5) Metz, R. B.; Neumark, D. M. *J. Chem. Phys.* **1992**, *97*, 962.
(6) Neumark, D. M. *Acc. Chem. Res.* **1993**, *26*, 33.
(7) Burnett, S. M.; Stevens, A. E.; Feigerle, C. S.; Lineberger, W. C. *Chem. Phys. Lett.* **1983**, *100*, 124.
(8) Ervin, K. M.; Ho, J.; Lineberger, W. C. *J. Chem. Phys.* **1989**, *91*, 5974.
(9) Wenthold, P. G.; Hrovat, D.; Borden, W. T.; Lineberger, W. C. *Science* **1996**, *272*, 1456.
(10) Wolf, S.; Sommerer, G.; Rutz, S.; Schreiber, E.; Leisner, T.; Woste, L.; Berry, R. S. *Phys. Rev. Lett.* **1995**, *74*, 4177.
(11) The term "NeNePo" is an abbreviation for the **Ne**gative ion−**Ne**utral atom−**Po**sitive ion charge reversal spectroscopy, as proposed by Wolf et al. (ref 10).
(12) Jeschke, H. O.; Garcia, M. E.; Bennemann, K. H. *J. Phys. B. Atom. Molec. Opt. Phys.* **1996**, *29*, L545.
(13) Jeschke, H. O.; Garcia, M. E.; Bennemann, K. H. *Phys. Rev. A* **1996**, *54*, R4601.
(14) Bersuker, I. B. *The Jahn−Teller Effect and Vibronic Interactions in Modern Chemistry*; Plenum Press: New York, 1984.
(15) Dobbyn, A. J.; Hutson, J. M. *J. Phys. Chem.* **1994**, *98*, 11428.
(16) Martins, J. L.; Car, R.; Buttet, J. *J. Chem. Phys.* **1983**, *78*, 5646.

(17) Berry, M. V. *Proc. R. Soc. (London), Ser. A* **1984**, *392*, 45.
(18) Gaus, J.; Kobe, K.; Bonacic-Koutecky, V.; Kuhling, H.; Manz, J.; Reischl, B.; Rutz, S.; Schreiber, E.; Woste, L. *J. Phys. Chem.* **1993**, *97*, 12509.
(19) Gomez Llorente, J. M.; Taylor, H. S. *J. Chem. Phys.* **1989**, *91*, 953.
(20) Morais, V. M. F.; Varandas, A. J. C. *J. Phys. Chem.* **1992**, *96*, 5704.
(21) Papanikolas, J. M.; Vorsa, V.; Nadal, M. E.; Campagnola, P. J.; Buchenau, H. K.; Lineberger, W. C. *J. Chem. Phys.* **1993**, *99*, 8733.
(22) Nadal, M. E.; Nandi, S.; Boo, D. W.; Lineberger, W. C. *J. Chem.* Phys., submitted for publication.
(23) Vorsa, V.; Campagnola, P. J.; Nandi, S.; Larsson, M.; Lineberger, W. C. *J. Chem. Phys.* **1996**, *105*, 2298.
(24) Balasubramanian, K.; Liao, M. Z. *Chem. Phys.* **1988**, *127*, 313.
(25) Balasubramanian, K.; Feng, P. Y. *Chem. Phys. Lett.* **1989**, *159*, 452.
(26) Basch, H. *J. Am. Chem. Soc.* **1981**, *103*, 4657.
(27) Bauschlicher Jr., C. W.; Langhoff, S. R.; Partridge, H. *J. Chem. Phys.* **1989**, *91*, 2412.
(28) Flad, J.; Igel-mann, G.; Preuss, H.; Stoll, H. *Chem. Phys.* **1984**, *90*, 257.
(29) Kaplan, I. G.; Santamaria, R.; Novaro, O. *Int. J. Quantum Chem. Symp.* **1993**, *27*, 743.
(30) Partridge, H.; Bauschlicher Jr., C. W.; Langhoff, S. R. *Chem. Phys. Lett.* **1990**, *175*, 531.
(31) Santamaria, R.; Kaplan, I. G.; Novaro, O. *Chem. Phys. Lett.* **1994**, *218*, 395.
(32) Walch, S. P.; Bauschlicher Jr., C. W.; Langhoff, S. R. *J. Chem. Phys.* **1986**, *85*, 5900.
(33) Walch, S. P. *J. Chem. Phys.* **1987**, *87*, 6776.
(34) Handschuh, H.; Cha, C. Y.; Bechthold, P. S.; Gantefor, G.; Eberhardt, W. *J. Chem. Phys.* **1995**, *102*, 6406.
(35) Bonacickoutecky, V.; Cespiva, L.; Fantucci, P.; Pittner, J.; Koutecky, J. *J. Chem. Phys.* **1994**, *100*, 490.
(36) Ho, J.; Ervin, K. M.; Lineberger, W. C. *J. Chem. Phys.* **1990**, *93*, 6987.
(37) Cheng, P. Y.; Duncan, M. A. *Chem. Phys. Lett.* **1988**, *152*, 341.
(38) LaiHing, K.; Cheng, P. Y.; Duncan, M. A. *Z. Phy. D—Atoms, Molecules and Clusters* **1989**, *13*, 161.
(39) Wedum, E. E.; Grant, E. R.; Cheng, P. Y.; Willey, K. F.; Duncan, M. A. *J. Chem. Phys.* **1994**, *100*, 6312.
(40) Fedrigo, S.; Harbich, W.; Buttet, J. *J. Chem. Phys.* **1993**, *99*, 5712.
(41) Harbich, W.; Fedrigo, S.; Meyer, F.; Lindsay, D. M.; Lignieres, J.; Rivoal, J. C.; Kreisle, D. *J. Chem. Phys.* **1990**, *93*, 8535.
(42) Calaminici, P.; Koster, A. M.; Russo, N.; Salahub, D. R. *J. Chem. Phys.* **1996**, *105*, 9546.